First experimental observation of vacancy assisted martensitic transformation shift in Ni-Fe-Ga alloys

I. Unzueta,[1,2,*] D. Alonso de R-Lorente,[3,†] E. Cesari,[4,‡] V. Sánchez-Alarcos,[3,5,§] V. Recarte,[3,5,¶] J. I. Pérez-Landazábal,[3,5,**] J. A. García,[6,2,††] and F. Plazaola[1,‡‡]

[1] *Department of Electricity and Electronics, University of the Basque Country UPV/EHU, 48940 Leioa, Spain*
[2] *BCMaterials, University of Basque Country UPV/EHU, 48940 Leioa, Spain*
[3] *Department of Science, Universidad Pública de Navarra, Campus de Arrosadía, 31006 Pamplona, Spain*
[4] *Department of Physics, Universitat de les Illes Balears, Ctra. de Valldemossa, km 7.5, E-07122, Palma de Mallorca, Spain*
[5] *Institute for Advanced Materials (INAMAT), Universidad Pública de Navarra, Campus de Arrosadía, 31006 Pamplona, Spain*
[6] *Department of Applied Physics II, University of the Basque Country UPV/EHU, 48940 Leioa, Spain*

Positron annihilation lifetime spectroscopy is used to experimentally demonstrate the direct relationship between vacancies and the shift of the martensitic transformation temperature in a $Ni_{55}Fe_{17}Ga_{28}$ alloy. The evolution of vacancies assisting the ordering enables shifts of the martensitic transformation up to 50 K. Our results confirm the role that both vacancy concentration and different vacancy dynamics play in samples quenched from the $L2_1$ and B2 phases, which dictate the martensitic transformation temperature and its subsequent evolution. Finally, by electron-positron density functional calculations V_{Ni} is identified as the most probable vacancy present in $Ni_{55}Fe_{17}Ga_{28}$. This work, evidences the capability of vacancies for the fine tuning of the martensitic transformation temperature, paving the way for defect engineering of multifunctional properties.

The plethora of multifunctional properties that Ni-based Ni_2YZ Heusler alloys display, such as giant magnetoresistance[1, 2], magnetocaloric effect[3, 4], large magnetic-field-induced strain[5, 6] and shape-memory effect[7] are linked to the occurrence of the so-called martensitic transformation (MT). MT is a first order diffusionless phase transformation based on electronic properties[8, 9] and driven by the Jahn-Teller splitting[10]. These promising features, however, are hindered by the poor mechanical properties that these alloys present[11]. In this context, Ni-Fe-Ga systems are increasingly attracting great interest due to their mechanical properties and its consequent enhanced deformation behavior[12–14]. The improved ductility performance in bulky off-stoichiometric samples makes the Ni-Fe-Ga system a promising alternative to the classic Ni-Mn-Ga alloys[15]. Recently, a giant reversible elastocaloric effect has been reported in Ni-Fe-Ga alloys near room temperature[16].

Hereby, the control of the MT and its related features acquire a key relevance for a proper optimization of the aforementioned functional properties. For instance, in Ni-Mn based Heusler alloys and in Ni-Fe-Ga systems, the composition[17] and doping[18, 19] are the main factors affecting the MT temperature (T_{MT}). In the Ni-Fe-Ga system, the composition can be tuned to get a T_{MT} near room temperature[20]. Additionally, the microstructure plays a key role on the MT characteristics[21]. The magnetism of Ni-Fe-Ga atoms is mainly confined to the Fe sites and the variation of Fe-Fe distances affects strongly the exchange coupling[22, 23]. Moreover, the degree of long-range atomic order is found to affect strongly both T_c Curie's temperature and T_{MT}, which in some Ni-Mn based alloys enables shifts of T_{MT} (ΔT_{MT}) of about 100 K[24].

Several works have considered the potential role of vacancies on MT. Ren and Otsuka[25, 26] demonstrate that the short-range atomic order during MT requires the diffusion of point defects to stabilize the MT. As vacancies assist the diffusion and the ordering process, they could also affect the MT. Indeed, Zhang *et al.*[27] speculate that vacancies could be the source of the observed entropy change in some Heusler Alloy ribbons. Other works point out the influence that vacancies may have on the pinning of MT[28–30]. In connection with the ordering process, Sánchez-Alarcos *et al.* and Santamarta *et al.* suggest different vacancy dynamics as responsible for the changes observed in T_c[31] and T_{MT}[32–34] in Ni-Mn-Ga and Ni-Fe-Ga alloys respectively. Hsu *et al.*[35] indicate that vacancies may drive the $L2_1 \rightarrow$ B2 order-disorder transition. However, none of the above suggestions have been experimentally proven, being the elusive nature of vacancies which has made it less experimentally investigated compared to other physical factors. As far as we know, there is no experimental proof of vacancies assisting the aforementioned processes in the literature.

The vast majority of works have been conducted within a theoretical framework, where formation energies of dif-

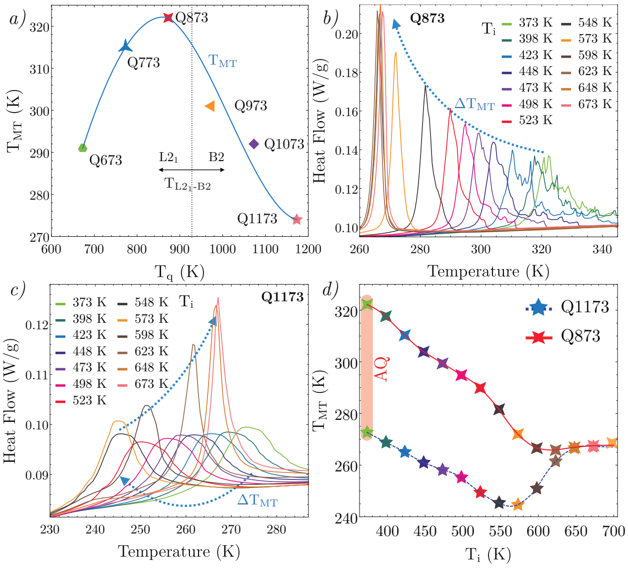

FIG. 1. (a) Direct T_{MT} versus T_q for all quenched samples. (b) Direct DSC curves for the 873 and (c) 1173 samples for each IAC. (d) The evolution of T_{MT} of Q873 and Q1173 samples as a function of the isochronal annealing temperature T_i.

ferent type of vacancy defects are calculated[36–40]. Recent works, by first principles calculations[41] and Monte Carlo simulations[42] link vacancies with the ordering process and their potential effect on T_{MT}. Regarding the experimental reports, the most complete study so far has been conducted by Merida *et al.*[43, 44] in Ni-Mn-Ga system by positron annihilation lifetime spectroscopy (PALS). However no evidence linking the vacancy concentration (C_v) and T_{MT} shift has been reported. In the present work, by combining PALS and Differential Scanning Calorimetry (DSC), it is experimentally demonstrated that there is a direct relationship between vacancies and ΔT_{MT} in $Ni_{55}Fe_{17}Ga_{28}$ alloy. It is also proven that the different evolution of T_{MT} exhibited by samples quenched from $L2_1$ or B2 phases is linked to different vacancy dynamics in each case. Besides, PALS measurements and Density Functional Theory (DFT) calculations point out that Ni vacancies are the most probable defects involved with ΔT_{MT}.

The synthesized $Ni_{55}Fe_{17}Ga_{28}$ polycrystalline samples (see Supplemental Material[45]) were quenched to ice water from temperatures ranging from 673 K up to 1173 K in 100 K steps. Samples are labeled according to their quenching temperature (T_q) as Q673K, Q773K, and so forth. The influence of T_q on T_{MT} has been evaluated by DSC measurements. As shown in Fig. 1(a), for samples quenched from $T_q < 900$ K, T_{MT} increases along with T_q increase. However, for samples with $T_q > 900$ K, T_{MT} decreases as T_q increases. In Ni-Mn based Heusler alloys and in Ni-Fe-Ga alloys, T_{MT} is highly sensitive to the atomic order[33, 46–48]. Indeed, as opposed to other Ni-Mn alloys[49], a less ordered $L2_1$ phase results in a higher T_{MT}[33, 50]. Thus, the observed increment of T_{MT} for the samples quenched from $T_q < 900$ K indicates that for higher T_q, the retained $L2_1$ order degree is lower. However, for samples quenched from $T_q > 900$ K, T_{MT} decreases with the increasing T_q, denoting a higher degree of $L2_1$ order retained during quenching.

The different dependencies of T_{MT} on T_q shown by the as-quenched (AQ) samples matches the occurrence of a second neighbor ordering transition at 930 K ($T_{L2_1\text{-}B2}$), see Fig. 1(a). Thereby, it implies that while Q673, Q773 and Q873 samples have been quenched within the same structure (from $L2_1$ to $L2_1$), samples Q973, Q1073 and Q1173 have been quenched from B2 phase to $L2_1$. Santamarta *et al.*[33, 51] and Oikawa *et al.*[34] ascribe the dependency that the evolution of T_{MT} has on T_q, to different C_v for the $L2_1$ and B2 phases, which would promote different long-range atomic order retained during quenching. Moreover, previous works on Fe-Ni systems also show the dependence of T_{MT} on T_q, which has been also ascribed to the presence of quenched-in vacancies[35]. However, none of the previous works contribute any experimental evidence supporting their claims.

As vacancies mediate the ordering process via diffusion[43], a different C_v could explain the observed phenomena. In this context, the powerful combination of PALS and DFT theory have been proven to be one of the most accurate techniques for the advanced characterization of vacancy defects in metals and semiconductors[52, 53]. Thus, in order to ascertain the potential role of vacancies on the T_{MT} shift, PALS experiments, along with theoretical positron lifetime calculations have been conducted on $Ni_{55}Fe_{17}Ga_{28}$ samples.

Fig. 2(a) shows the experimental average positron lifetime values ($\overline{\tau}$) for samples Q1173 and Q873. As discussed in Supplemental Material[45], spectra could not be decomposed because $\overline{\tau}$ is in a saturation trapping

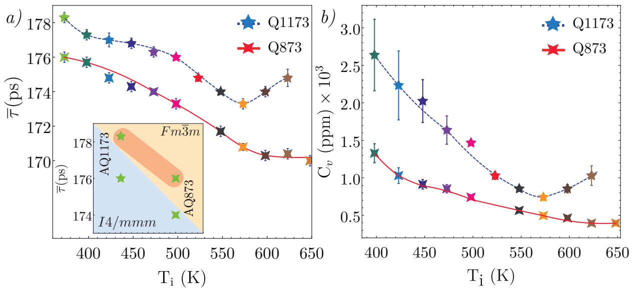

FIG. 2. PALS measurements of the samples quenched above (Q1173), and below (Q873) $T_{L2_1\text{-}B2}$. (a) shows the measured $\overline{\tau}$ and (b) the corresponding C_v calculated by means of Eq. (1) with $\tau_b = 106$ ps and $\tau_v = 178$ ps. The inset in (a) show the $\overline{\tau}$ values of AQ1173 and AQ873 samples measured in both, austenite ($Fm\bar{3}m$, yellow region) and martensite ($I4/mmm$, blue region) phases.

regime[54]. Anywise, for a given defect (one positron trap), $\overline{\tau}$ only depends on C_v, and the relation between $\overline{\tau}$ and C_v is given by the so-called *one-trap model*[45]

$$C_v = \frac{1}{\tau_b \mu_v} \frac{\overline{\tau} - \tau_b}{\tau_v - \overline{\tau}}, \qquad (1)$$

where $\mu_v = 1.5 \times 10^{14}\mathrm{s}^{-1}$[43, 44, 55, 56] is the specific trapping rate, $\tau_b = 106$ ps the theoretically calculated bulk lifetime (see Table I) and $\tau_v = 178$ ps (see Fig. 2(a)). As inferred from Eq. (1) and evidenced in Fig. 2(b), a larger $\overline{\tau}$ implies a larger C_v.

The inset of Fig. 2(a) shows $\overline{\tau}$ values of AQ Q1173 (AQ1173) and AQ Q873 (AQ873) samples measured in both, austenite ($Fm\overline{3}m$, yellow region) and martensite ($I4/mmm$, blue region) phases. As indicated by the area shaded in red, the $\overline{\tau}$ value of sample AQ1173 measured in the $Fm\overline{3}m$ phase is higher than the one of AQ873. The same trend is observed for samples AQ1173 and AQ873 measured in the $I4/mmm$ phase, indicating that the B2 phase is characterized by larger C_v than the $L2_1$ phase. A larger C_v results in a larger supply of vacancies, which assist more effectively the ordering process during quenching. The larger C_v gives rise to an enhanced degree of $L2_1$ order degree in sample AQ1173, which explains the lower T_{MT} that AQ1173 exhibits compared to AQ873 sample (see Fig. 1(a) and the area shaded in red of Fig. 1(d)).

In order to study the vacancy dynamics in samples quenched above and below the $T_{L2_1\text{-}B2}$, AQ samples were subjected to isochronal annealing cycles (IAC). IAC consists on heating up the samples up to a maximum temperature (T_i) (from 398 K to 698 K every 25 K) at a constant rate of 10 K/min. Then, after reaching T_i samples are cooled down at the same rate to the initial temperature. Fig. 2 shows the evolution of both $\overline{\tau}$ and C_v (which inherits the same evolution of $\overline{\tau}$), as a function of T_i for Q873 and Q1173 samples. The most outstanding fact is the different behavior of $\overline{\tau}$ (and C_v) for Q1173 and Q873 in respect to T_i. For sample Q873 C_v decreases monotonically with T_i increase, while for sample Q1173 C_v decreases until $T_i \approx 570$ K. Then, from that temperature on, C_v increases as T_i does, indicating different vacancy dynamics for samples quenched above and below $T_{L2_1\text{-}B2}$.

For the sake of comparison, the evolution of T_{MT} is also tracked by means of IAC. Fig. 1(b) and 1(c) show a detailed shape of the DSC thermogram peaks for samples Q873K and Q1173K respectively. In sample Q873K T_{MT} decreases monotonically with increasing T_i. However, T_{MT} for sample Q1173 initially decreases with T_i increase, but above $T_i \approx 570$ K, T_{MT} increases along with T_i. In fact, the same behavior is reproduced for all the samples with $T_q < T_{L2_1\text{-}B2}$ and $T_q > T_{L2_1\text{-}B2}$(see Ref. [45]). In a nutshell, as shown in Fig. 1(d), the shift of T_{MT} also shows a different behaviour depending on whether the sample is quenched above or below the $T_{L2_1\text{-}B2}$ temperature. Additionally, the evolution of C_v in respect to T_i matches with the evolution of T_{MT} respect to T_i, which suggest that different vacancy dynamics may play a role on the dependency that the shift of T_{MT} shows on T_q(see Fig. 1 and Fig. 2).

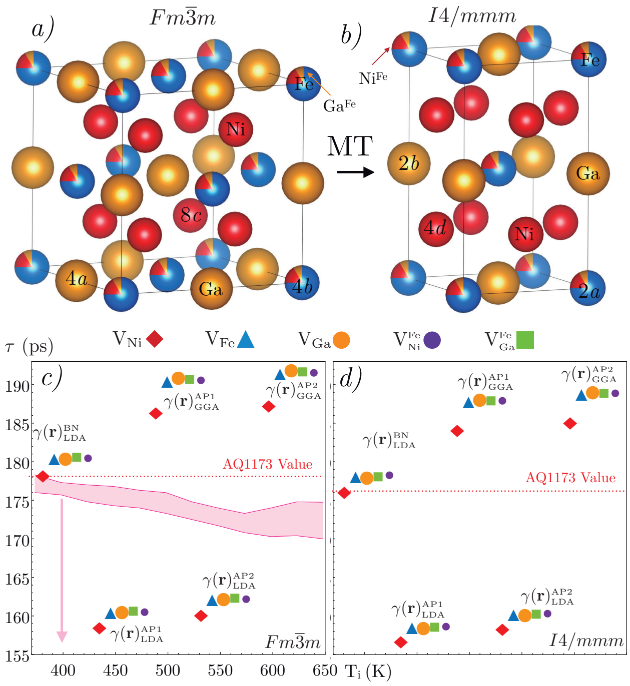

FIG. 3. Illustration of the (a) austenite and (b) martensite phases of Ni-Fe-Ga alloy. The calculated defect-related characteristic lifetimes for several possible type of vacancies, as well as for five different parameterization of $\gamma(\mathbf{r})$ (c) for $Fm\overline{3}m$ phase, and (d), for $I4/mmm$ phase. The red-dashed lines indicate experimental AQ $\overline{\tau}$ values. The red shadowed area illustrates the experimentally measured $\overline{\tau}$ range in the austenite phase.

In order to complement the experimental PALS results, DFT calculations of the positron lifetime in $Ni_{55}Fe_{17}Ga_{28}$ alloy were performed using the Atomic Superposition method[57], which provides satisfactory values for metals and semiconductors[58–60]. Positron lifetime calculations were performed for exact $Ni_{55}Fe_{17}Ga_{28}$ composition, where the excess Ni and Ga atoms have been placed in Fe positions[61, 62]. By overlapping the $n_+(\mathbf{r})$ positron density with the $n_-(\mathbf{r})$ electron density of the $Ni_{55}Fe_{17}Ga_{28}$, the annihilation rate $\lambda = \tau^{-1}$ was evaluated by

$$\lambda = \tau^{-1} = \pi c r_0^2 \int n_+(\mathbf{r}) n_-(\mathbf{r}) \gamma(\mathbf{r}) \mathrm{d}\mathbf{r} \qquad (2)$$

where c is the speed of light in vacuum, r_0 the classical electron radius and $\gamma(\mathbf{r})$ the so-called enhancement factor that comprises the enhanced electron density due to the positron Coulombic attraction. $n_-(\mathbf{r})$ has been constructed by adding individual atomic charge densities around $\mathbf{R}_i$ atomic positions for the perfect lattice (bulk) and defected lattice, with different type of possible vacancies. In off-stoichiometric conditions, the excess Ni and Ga occupy the Fe sites[61, 62], thus leading to two non-equivalent positions of both Ni and Ga, and a single Fe position (see Fig. 3(a) and 3(b)). As a consequence, five types of vacancy defects are possible; V_{Ni}, V_{Fe} and V_{Ga}, and vacancies of antisite atoms V_{Ni}^{Fe} and V_{Ga}^{Fe}. The last vacancies refer to vacancies of antisite Ga and Ni excess atoms occupying natural Fe positions[61, 62]. Calculations were carried out in unrelaxed $Fm\bar{3}m$ and $I4/mmm$ structures. Table I gathers the crystallographic data of the structures used in the calculations[45].

The enhancement factor $\gamma(\mathbf{r})$ of Eq. (2) has been modeled within the Local Density (LDA) and Generalized Gradient (GGA) Approximations using five different parameterizations, labeled $\gamma(\mathbf{r})^{\rm BN}_{\rm LDA}$, $\gamma(\mathbf{r})^{\rm AP1}_{\rm LDA}$, $\gamma(\mathbf{r})^{\rm AP2}_{\rm LDA}$, $\gamma(\mathbf{r})^{\rm AP1}_{\rm GGA}$ and $\gamma(\mathbf{r})^{\rm AP2}_{\rm GGA}$ (for exact expressions see the Supplemental Material[45]). Results of the calculated defect-related positron lifetimes are illustrated in Fig. 3(c) and 3(d) respectively. The area shaded in red indicates the range of experimental $\overline{\tau}$ values. Calculated bulk lifetimes are not explicitly shown since in all cases τ_b ranges between 100 - 130 ps. Thus, in order to explain the experimental $\overline{\tau}$ of Fig. 2, a vacancy-type defect must be considered[45].

Regardless of the phase and the parameterization used, the calculated lifetime of V_{Ni} is slightly lower compared to the other ones. Depending on the $\gamma(\mathbf{r})$ parameterization, a clear dispersion is observed. On the one hand, by comparing the shaded area in Fig. 3(c) and the theoretical calculations, it is concluded that $\gamma(\mathbf{r})^{\rm AP1}_{\rm LDA}$ and $\gamma(\mathbf{r})^{\rm AP2}_{\rm LDA}$ underestimate the positron lifetime. These characteristic lifetimes cannot reproduce the experimental values because of the $\overline{\tau} \leq \tau_v$ constraint[45]. On the other hand, $\gamma(\mathbf{r})^{\rm AP1}_{\rm GGA}$ and $\gamma(\mathbf{r})^{\rm AP2}_{\rm GGA}$ yield values up to $\approx$ 12 ps higher than the experimental ones.

As previously commented, the evolution of the experimental $\overline{\tau}$ is in the saturation trapping regime. In this regime, the contribution of the saturated defect overcomes the bulk contribution and $\overline{\tau}$ reflects the characteristic lifetime that the defect present, $\overline{\tau} \approx \tau_v$[45, 54]. Along with it, the highest value that has been reached by quenching has always been around 178 ps. Therefore the $\gamma(\mathbf{r})^{\rm BN}_{\rm LDA}$ parameterization is the one that predicts best the experimental results[63].

The last column of Table I gathers the calculated positron lifetimes using $\gamma(\mathbf{r})^{\rm BN}_{\rm LDA}$. It is worth mentioning that PALS measurements of samples Q1173 and Q873 during IAC were taken at 350 K ($Fm\bar{3}m$ phase). The calculated positron lifetime value of V_{Ni} is the one that best matches sample AQ1173's experimental value, that is 178 ps (see Fig. 3(c)). Additionally, prior to IAC, both quenched samples were also measured in the $I4/mmm$ phase at 273 K, showing a value of 176 ps for AQ1173 and 174 ps for AQ873 (see Fig. 2, inset, blue shadowed area). As shown in Fig. 3(d), the 176 ps value matches with the calculated value of V_{Ni} in $I4/mmm$ phase. As a result, the vacancy concentration for AQ1173 is higher than for the one for AQ873 in both phases, as AQ873 shows values below 178 ps in the $Fm\bar{3}m$ and 176 ps in the $I4/mmm$. These results are in good agreement with most predictions of vacancy formation energies in Ni-based Heusler alloys[36–38, 40, 42], which indicate that Ni is the vacancy that presents the lowest formation energy, ranging between 0.4 - 0.7 eV. Therefore, it can be concluded that V_{Ni} is the most probable vacancy type defect assisting the observed shift in T_{MT}. However, the recently proposed parametrizations for $\gamma(\mathbf{r})$ [64, 65] may shed further proof of the vacancy-type defect present in $Ni_{55}Fe_{17}Ga_{28}$.

Phase	Cell parameters			τ_v
Ref. [62]	Atom	Site	Occupancy	$\gamma(\mathbf{r})^{\rm BN}_{\rm LDA}$
	V_{Ni}	$8c$ (1/4,1/4,1/4)	1.00	178 ps
Austenite	V_{Ni}^{Fe}	$4a$ (0,0,0)	0.16	180 ps
$Fm\bar{3}m$, 225	V_{Ga}	$4b$ (1/2,1/2,1/2)	1.00	181 ps
$a = 5.774$Å	V_{Ga}^{Fe}	$4a$ (0,0,0)	0.08	180 ps
	V_{Fe}	$4a$ (0,0,0)	0.76	181 ps
	Bulk	(—)	(—)	106 ps
	V_{Ni}	$4d$ (0,1/2,1/4)	1.00	176 ps
Martensite	V_{Ni}^{Fe}	$2a$ (0,0,0)	0.16	178 ps
$I4/mmm$, 139	V_{Ga}	$2b$ (0,0,1/2)	1.00	178 ps
$a = b = 5.818$Å	V_{Ga}^{Fe}	$2a$ (0,0,0)	0.08	178 ps
$c = 6.49600$	V_{Fe}	$2a$ (0,0,0)	0.76	178 ps
	Bulk	(—)	(—)	104 ps

Table I. Structural parameters used in theoretical calculations. The last column gathers the theoretical defect-related positron lifetime values calculated by $\gamma(\mathbf{r})^{\rm BN}_{\rm LDA}$ parameterization.

Finally, taking into account the good agreement between experimental PALS results and DFT calculations, C_v values for samples Q873 and Q1173 can be calculated by means of Eq. (1) using τ_b = 106 ps and τ_v = 178 ps, see Fig. 2(b). Further more, Fig. 4 evidences the mutual dependence of the evolution of T_{MT} and C_v. It is important to notice that the variation of T_{MT} (the recovery of the $L2_1$ order-degree assisted by vacancies) is relative to the retained $L2_1$ order-degree of the AQ samples. The underlying mechanism by which vacancies drive the ΔT_{MT} may be related to the interaction of vacancies with partial dislocations[35] or vacancies acting as pinning centers[30, 66], among others. In particular, Ren and Otsuka [25, 26] demonstrate that for the short-range order adaptation between phases, the aging of the sample is needed, which opens a time lag for vacancies to accommodate. The diffusion of point defects to match the new symmetry may be a plausible mechanism by which the MT characteristics are altered. Anyway, as shown by Fig. 4, the present results clearly prove that vacancies play a fundamental role on ΔT_{MT}.

In sample Q1173, the ordering process during subsequent IAC is accomplished by a reduction of C_v (Fig. 4(a)), which in turn, matches the T_{MT} decrease (see Fig. 1(c) and 1(d)), enhancing the degree $L2_1$ order with the consequent decrease of T_{MT}. Additionally, as shown in the inset of Fig. 4(a), between 550 - 600 K, T_{MT} increases with C_v increase. Indeed, the increase of C_v and the increase of T_{MT} take place at the same temperature and the inset shows their correlated evolution.

Regarding sample AQ873, the same behavior is observed. During IAC, T_{MT} decreases monotonically rather than showing a minimum value as C_v does in Q1173. Even so, the vacancy dynamics of sample Q873 follows the same trend of T_{MT}. Fig. 4(b) shows their mutual dependence and again, the shift of T_{MT} is directly related with the evolution of C_v. The different evolution that C_v shows in samples Q1173 and Q873 evidences different vacancy dynamics in samples quenched above or below $T_{L2_1\text{-}B2}$, which results in a different evolution of T_{MT}. However, the mutual dependence of C_v and T_{MT} in both samples do confirm that vacancies play a fundamental role in the evolution of T_{MT}.

In conclusion, we demonstrate experimentally for the first time that vacancies assist the shift of T_{MT}. DSC measurements enable the tracking of T_{MT}, whereas PALS reveals its dependency on C_v. Thereby, the longstanding question of whether the different T_{MT} evolution for samples quenched above or below $T_{L2_1\text{-}B2}$ rely on different vacancy dynamics, is answered. Additionally, electron-positron DFT calculations enable the identification of V_{Ni} as the most probable vacancy in the $Ni_{55}Fe_{17}Ga_{28}$ alloy. In summary, this work shows the potential of vacancies for the fine tuning of T_{MT}, enabling shifts in up to $\approx$ 50 K. This work opens the way for defect engineering in tuning T_{MT} and the related multifunctional properties of Ni-Fe-Ga alloys.

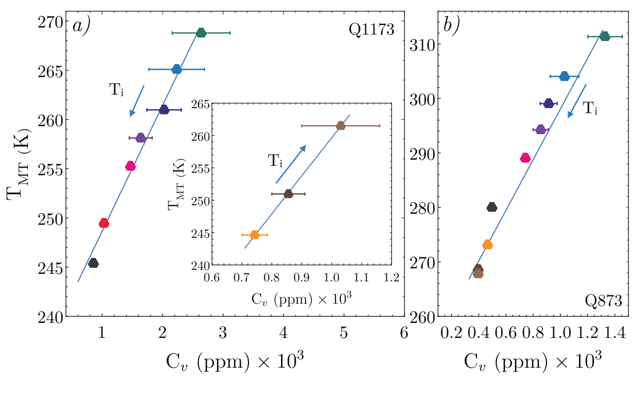

FIG. 4. (a) C_v vs T_{MT} for the Q1173 sample. For a better display, the range in which both T_{MT} and C_v increases are shown in the inset. (b) Dependence of C_v and T_{MT} for the Q873 sample. Both curves manifest the mutual dependence between vacancies and ΔT_{MT}.

This work is supported for the Basque Government Grant IT-1005-16 and by the Spanish Ministry of Economy and Competitiveness under the projects MAT2015-65165-C2-R (MINECO/FEDER), MAT2014-56116-C4-1-R and GIC1585. I. Unzueta wants to acknowledge the Basque Government Grant PRE-2014-214.

* iraultza.unzueta@ehu.eus
† d˙alonso60@hotmail.com
‡ eduard.cesari@uib.cat
§ vicente.sanchez@unavarra.es
¶ recarte@unavarra.es
** ipzlanda@unavarra.es
†† joseangel.garcia@ehu.eus
‡‡ fernando.plazaola@ehu.eus

[1] S. Y. Yu, Z. H. Liu, G. D. Liu, J. L. Chen, Z. X. Cao, G. H. Wu, B. Zhang, and X. X. Zhang, Appl. Phys. Lett. **89**, 162503 (2006).
[2] S. Banik, R. Rawat, P. K. Mukhopadhyay, B. L. Ahuja, A. Chakrabarti, P. L. Paulose, S. Singh, A. K. Singh, D. Pandey, and S. R. Barman, Phys. Rev. B **77**, 224417 (2008).
[3] A. Planes, L. Mañosa, and M. Acet, J. Phys. Condens. Matter **21**, 233201 (2009).
[4] L. Mañosa, D. González-Alonso, A. Planes, E. Bonnot, M. Barrio, J.-L. Tamarit, S. Aksoy, and M. Acet, Nat. Mater. **9**, 478 EP (2010).
[5] K. Ullakko, J. K. Huang, C. Kantner, R. C. O'Handley, and V. V. Kokorin, Appl. Phys. Lett. **69**, 1966 (1996).
[6] M. Chmielus, X. X. Zhang, C. Witherspoon, D. C. Dunand, and P. Müllner, Nat. Mater. **8**, 863 EP (2009).
[7] Y. Sutou, Y. Imano, N. Koeda, T. Omori, R. Kainuma, K. Ishida, and K. Oikawa, Appl. Phys. Lett. **85**, 4358 (2004).
[8] M. Ye, A. Kimura, Y. Miura, M. Shirai, Y. T. Cui, K. Shimada, H. Namatame, M. Taniguchi, S. Ueda, K. Kobayashi, R. Kainuma, T. Shishido, K. Fukushima, and T. Kanomata, Phys. Rev. Lett. **104**, 176401 (2010).
[9] E. Şaşıoğlu, L. M. Sandratskii, and P. Bruno, Phys. Rev. B **77**, 064417 (2008).
[10] S. Fujii, S. Ishida, and S. Asano, J. Phys. Soc. Jpn. **58**, 3657 (1989).
[11] C. Tan, Z. Tai, K. Zhang, X. Tian, and W. Cai, Sci. Rep. **7**, 43387 EP (2017).
[12] P. Álvarez-Alonso, C. Aguilar-Ortiz, E. Villa, A. Nespoli, H. Flores-Zúñiga, and V. Chernenko, Scr. Mater. **128**, 36 (2017).
[13] Y. Xu, B. Lu, W. Sun, A. Yan, and J. Liu, Appl. Phys. Lett. **106**, 201903 (2015), https://doi.org/10.1063/1.4921531.
[14] S. Chabungbam, P. Borgohain, S. Ghosh, N. Singh, and M. B. Sahariah, J. Alloy. Comp. **689**, 199 (2016).
[15] J. Pons, E. Cesari, C. Seguí, F. Masdeu, and R. Santamarta, Mater. Sci. Eng. A **481-482**, 57 (2008), proceedings of the 7th European Symposium on Martensitic Transformations, ESOMAT 2006.

[16] Y. Li, D. Zhao, and J. Liu, Sci. Rep. **6**, 25500 EP (2016).
[17] S. Chabungbam, S. Gowtham, and M. B. Sahariah, Phys. Rev. B **89**, 085114 (2014).
[18] K. Oikawa, Y. Imano, V. A. Chernenko, F. Luo, T. Omori, Y. Sutou, R. Kainuma, T. Kanomata, and K. Ishida, Mater. Trans. **46**, 734 (2005).
[19] H. Morito, A. Fujita, K. Oikawa, K. Fukamichi, R. Kainuma, T. Kanomata, and K. Ishida, J. Phys. Condens. Matter **21**, 076001 (2009).
[20] K. Oikawa, T. Ota, T. Ohmori, Y. Tanaka, H. Morito, A. Fujita, R. Kainuma, K. Fukamichi, and K. Ishida, Appl. Phys. Lett. **81**, 5201 (2002).
[21] H. R. Zhang, C. Ma, H. F. Tian, G. H. Wu, and J. Q. Li, Phys. Rev. B **77**, 214106 (2008).
[22] Z. H. Liu, H. N. Hu, G. D. Liu, Y. T. Cui, M. Zhang, J. L. Chen, G. H. Wu, and G. Xiao, Phys. Rev. B **69**, 134415 (2004).
[23] Y. Qawasmeh and B. Hamad, J. Appl. Phys. **111**, 033905 (2012).
[24] V. Recarte, J. Pérez-Landazábal, V. Sánchez-Alarcos, and J. Rodríguez-Velamazán, Acta Mater. **60**, 1937 (2012).
[25] X. Ren and K. Otsuka, Nature **389**, 579 EP (1997).
[26] X. Ren and K. Otsuka, Phys. Rev. Lett. **85**, 1016 (2000).
[27] Y. Zhang, L. Zhang, Q. Zheng, X. Zheng, M. Li, J. Du, and A. Yan, Sci. Rep. **5**, 11010 EP (2015).
[28] Z. ni Zhou, L. Yang, J. ge Wang, T. Jin, Y. Huang, J. Li, Q. Hu, and J. guo Li, Prog. Nat. Sci-Mater. **27**, 356 (2017).
[29] S. Kustov, J. Pons, E. Cesari, and J. V. Humbeeck, Acta Mater. **52**, 3075 (2004).
[30] S. Kustov, J. Pons, E. Cesari, and J. V. Humbeeck, Acta Mater. **52**, 3083 (2004).
[31] V. Sánchez-Alarcos, V. Recarte, J. Pérez-Landazábal, and G. Cuello, Acta Mater. **55**, 3883 (2007).
[32] J. Font, J. Muntasell, R. Santamarta, J. Pons, E. Cesari, V. Recarte, J. Pérez-Landazábal, C. Gómez-Polo, and J. Dutkiewicz, Mater. Sci. Eng. A **481-482**, 262 (2008), proceedings of the 7th European Symposium on Martensitic Transformations, ESOMAT 2006.
[33] R. Santamarta, E. Cesari, J. Font, J. Muntasell, J. Pons, and J. Dutkiewicz, Scr. Mater. **54**, 1985 (2006).
[34] K. Oikawa, T. Omori, Y. Sutou, H. Morito, R. Kainuma, and K. Ishida, Metall. Materi. Trans. A **38**, 767 (2007).
[35] T. Y. Hsu and Y. Linfah, J. Mater. Sci. **18**, 3213 (1983).
[36] J. Bai, J. M. Raulot, Y. D. Zhang, C. Esling, X. Zhao, and L. Zuo, J. Appl. Phys. **108**, 064904 (2010).
[37] J. Bai, N. Xu, J.-M. Raulot, Y. D. Zhang, C. Esling, X. Zhao, and L. Zuo, J. Appl. Phys **113**, 174901 (2013).
[38] J. Bai, N. Xu, J. M. Raulot, C. Esling, X. Zhao, and L. Zuo, Int. J. Quantum Chem **113**, 847.
[39] S. Kulkova, S. Eremeev, S. Kulkov, and V. Skripnyak, Mat. Sci. Eng. A **481-482**, 209 (2008), proceedings of the 7th European Symposium on Martensitic Transformations, ESOMAT 2006.
[40] S. Kulkova, S. Eremeev, Q. Hu, C. Li, and R. Yang, in *ESOMAT 2009 (Czech Republic, September 7-11, 2009)*, 02017 (EDP Sciences, Les Ulis,France, 2009).
[41] A. Kosogor, V. V. Sokolovskiy, V. A. L'vov, and V. V. Khovaylo, Phys. Status Solidi B **252**, 2309 (2015).
[42] Y. Wang, D. Salas, B. Medasani, P. Entel, I. Karaman, R. Arróyave, and T. C. Duong, Phys. Status Solidi B **255**, 1700523 (2018).
[43] D. Merida, J. García, V. Sánchez-Alarcos, J. Pérez-Landazábal, V. Recarte, and F. Plazaola, J. Alloy. Comp **639**, 180 (2015).
[44] D. Merida, J. A. García, V. Sánchez-Alarcos, J. I. Pérez-Landazábal, V. Recarte, and F. Plazaola, Appl. Phys. Lett. **104**, 231905 (2014).
[45] See Supplemental Material at *link* for details of the synthesis and PALS experiments, for the exact expressions used in the modeling of $\gamma(\mathbf{r})$, and for the determination of vacancy concentration from the experimentally measured average positron lifetime. Also includes Refs. [67–85].
[46] V. Sánchez-Alarcos, J. I. Pérez-Landazábal, V. Recarte, J. A. Rodríguez-Velamazán, and V. A. Chernenko, J. Phys. Condens. Matter **22**, 166001 (2010).
[47] V. Sánchez-Alarcos, V. Recarte, J. Pérez-Landazábal, C. Gómez-Polo, and J. Rodríguez-Velamazán, Acta Mater. **60**, 459 (2012).
[48] V. Sánchez-Alarcos, J. Pérez-Landazábal, V. Recarte, I. Lucia, J. Vélez, and J. Rodríguez-Velamazán, Acta Mater. **61**, 4676 (2013).
[49] V. Sánchez-Alarcos, J. Pérez-Landazábal, C. Gómez-Polo, and V. Recarte, J. Magn. Magn. Mater **320**, e160 (2008).
[50] C. Picornell, J. Pons, E. Cesari, and J. Dutkiewicz, Intermetallics **16**, 751 (2008).
[51] R. Santamarta, J. Font, J. Muntasell, F. Masdeu, J. Pons, E. Cesari, and J. Dutkiewicz, Scr. Mater **54**, 1105 (2006), viewpoint set no. 40: Grain boundary engineering.
[52] P. Hautöjarvi, *Positrons in Solids. Topics in Current Physics*, Vol. 12 (Springer, Heidelberg, 1979).
[53] B. Barbiellini in *New Directions in Antimatter Chemistry and Physics* edited by C. M. Surko and F. A. Gianturco (Kluwer Academic Publishers, Dordrecht, 2001), p. 127.
[54] F. Tuomisto and I. Makkonen, Rev. Mod. Phys. **85**, 1583 (2013).
[55] T. E. M. Staab, R. Krause-Rehberg, B. Vetter, and B. Kieback, J. Phys. Condens. Matter **11**, 1807 (1999).
[56] H.-E. Schaefer, Phys. Status Solidi A **102**, 47 (1987).
[57] M. J. Puska and R. M. Nieminen, J. Phys. F: Met. Phys. **13**, 333 (1983).
[58] B. Barbiellini, M. J. Puska, T. Korhonen, A. Harju, T. Torsti, and R. M. Nieminen, Phys. Rev. B **53**, 16201 (1996).
[59] T. Korhonen, M. J. Puska, and R. M. Nieminen, Phys. Rev. B **54**, 15016 (1996).
[60] I. Unzueta, N. Zabala, V. Marín-Borrás, V. Muñoz Sanjosé, J. A. García, and F. Plazaola, Phys. Rev. B **94**, 014117 (2016).
[61] J. Bai, Y. Chen, Z. Li, P. Jiang, P. Wei, and X. Zhao, AIP Adv. **6**, 125007 (2016).
[62] P. J. Brown, A. P. Gandy, K. Ishida, R. Kainuma, T. Kanomata, H. Morito, K.-U. Neumann, K. Oikawa, and K. R. A. Ziebeck, J. Phys. Condens. Matter **19**, 016201 (2007).
[63] I. Unzueta, V. Sánchez-Alarcos, V. Recarte, J. I. Pérez-Landazábal, N. Zabala, J. A. García, and F. Plazaola, Phys. Rev. B **99**, 064108 (2019).
[64] B. Barbiellini and J. Kuriplach, Phys. Rev. Lett. **114**, 147401 (2015).
[65] N. D. Drummond, P. López Ríos, R. J. Needs, and C. J. Pickard, Phys. Rev. Lett. **107**, 207402 (2011).
[66] A. Mansouri Tehrani, H. Shahrokhshahi, N. Parvin, and J. Brgoch, J. Appl. Phys. **118**, 014901 (2015).
[67] J. M. Barandiarán, V. A. Chernenko, P. Lázpita,

J. Gutiérrez, and J. Feuchtwanger, Phys. Rev. B **80**, 104404 (2009).
[68] P. Kirkegaard and M. Eldrup, Comput. Phys. Commun. **7**, 401 (1974).
[69] M. Bertolaccini and L. Zappa, Il Nuovo Cimento B Series 10 **52**, 487 (1967).
[70] B. Somieski, T. Staab, and R. Krause-Rehberg, Nucl. Instrum. Method. A. **381**, 128 (1996).
[71] K. Plotkowski, T. Panek, and J. Kansy, Il Nuovo Cimento D **10**, 933 (1988).
[72] I. MacKenzie and J. Fabian, Il Nuovo Cimento B **58**, 162 (1980).
[73] R. M. Nieminen, E. Boronski, and L. J. Lantto, Phys. Rev. B **32**, 1377 (1985).
[74] E. Boroński and R. M. Nieminen, Phys. Rev. B **34**, 3820 (1986).
[75] J. Arponen and E. Pajanne, Ann. Physics **121**, 343 (1979).
[76] L. J. Lantto, Phys. Rev. B **36**, 5160 (1987).
[77] B. Barbiellini, M. J. Puska, T. Torsti, and R. M. Nieminen, Phys. Rev. B **51**, 7341 (1995).
[78] J. M. C. Robles, E. Ogando, and F. Plazaola, J. Phys. Condens. Matter **19**, 176222 (2007).
[79] G. E. Kimball and G. H. Shortley, Phys. Rev. **45**, 815 (1934).
[80] W. Brandt and R. Paulin, Phys. Rev. B **5**, 2430 (1972).
[81] M. Puska and R. Nieminen, Rev. Mod. Phys. **66**, 841 (1994).
[82] K. Saarinen, P. Hautojärvi, A. Vehanen, R. Krause, and G. Dlubek, Phys. Rev. B **39**, 5287 (1989).
[83] C. Corbel, F. Pierre, K. Saarinen, P. Hautojärvi, and P. Moser, Phys. Rev. B **45**, 3386 (1992).
[84] F. Plazaola, K. Saarinen, L. Dobrzynski, H. Reniewicz, F. Firszt, J. Szatkowski, H. Meczynska, S. Legowski, and S. Chabik, J. Appl. Phys. **88**, 1325 (2000).
[85] R. Krause-Rehberg, A. Polity, W. Siegel, and G. Kuhnel, Semicond. Sci. Tech. **8**, 290 (1993).

Supplemental material for "First experimental observation of vacancy assisted martensitic transformation shift in Ni-Fe-Ga alloys"

I. Unzueta,[1,2,*] D. A. Robador-Lorente,[3] E. Cesari,[4] V. Sánchez-Alarcos,[3,5] V. Recarte,[3,5] J. I. Pérez-Landazábal,[3,5] J. A. García,[6,2] and F. Plazaola[1]

[1] *Department of Electricity and Electronics, University of the Basque Country UPV/EHU, 48940 Leioa, Spain*
[2] *BCMaterials, University of Basque Country UPV/EHU, 48940 Leioa, Spain*
[3] *Department of Science, Universidad Pública de Navarra, Campus de Arrosadía, 31006 Pamplona, Spain*
[4] *Department of Physics, Universitat de les Illes Balears, Ctra. de Valldemossa, km 7.5, E-07122, Palma de Mallorca, Spain*
[5] *Institute for Advanced Materials (INAMAT), Universidad Pública de Navarra, Campus de Arrosadía, 31006 Pamplona, Spain*
[6] *Department of Applied Physics II, University of the Basque Country UPV/EHU, 48940 Leioa, Spain*

(Dated: April 2, 2019)

I Experimental details

Starting from high purity elements Ni, Fe and Ga, a polycrystalline ingot was cast by induction melting method under protective Ar atmosphere. The ingot was remelted several times to ensure homogeneity. After encapsulating the ingot in a quartz ampoule it was homogenized during 24 h at 1423 K in Ar atmosphere, followed by slow cooling in the furnace. Composition and the characteristic temperatures T_c and T_{MT} were measured by EDX and DSC respectively in a $Ni_{55}Fe_{17}Ga_{28}$ sample with $T_c \approx T_{MT} \approx$ 300 K[1]. The samples studied were quenched in ice water from 673 K to 1173 K in 100 K steps. Samples are labeled according to their quenching temperature T_q as Q673K, Q773K, Q873, Q973 Q1073 and Q1173.

Differential Scanning Calorimetry (DSC) measurements were carried out in a TA-Q100 at a heating/cooling rate of 10 K/min, from which the evolution of the direct T_{MT} was obtained for all samples. These values are gathered in Fig .1.

PALS experiments were performed using a fast-fast timing coincidence spectrometer with a FWHM resolution of 250 ps. The detectors are equipped with plastic scintillators from Saint-Gobain (BC-422) and Hamamatsu photomultiplier tubes (H1949-50) in a collinear geometry. All PALS spectra related to isochronal annealing cycles (IAC) were taken at 350 K (austenite phase, $Fm\bar{3}m$) and the as quenched samples were also measured in the martensite ($I4/mmm$) phase. Spectra were measured using a 15 μCi ^{22}NaCl positron source encapsulated between 7.5 μm Kapton foils and sandwiched by a pair of identical Ni-Fe-Ga samples. Each PALS spectrum was collected with more than 3×10^6 counts and analyzed with the POSITRONFIT code[2].

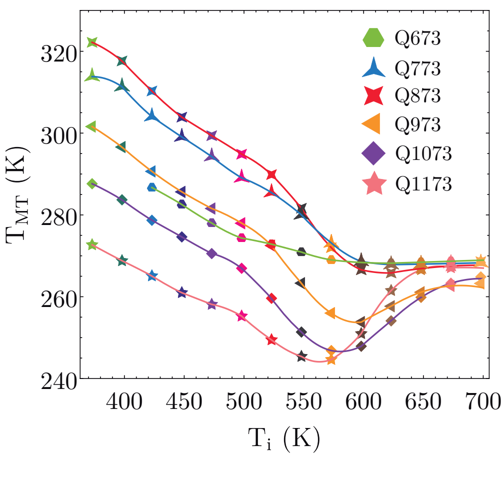

FIG. 1. The evolution of T_{MT} for all samples as a function of T_i.

All spectra were analyzed after subtracting the source contribution, which consists of two components. The lifetime related with the first component is around 1500 ps[3, 4] and the measured intensity was about 1%. The second component is related to the positron annihilation in Kapton which has a well-known value of 382 ps[5, 6]. The intensity of the former component that minimizes the χ^2 in all spectra was %13. In order to improve the accuracy of the PALS measurements, each point was measured up to 6 times. In all the measured points the error of $\overline{\tau}$ has been always below 0.5 ps.

Initially, the $Ni_{55}Fe_{17}Ga_{28}$ sample was slowly cooled from 1173 K, at a cooling rate of 0.3 K/min to 350 K. The sample was then measured by PALS at 350 K (to keep it in austenite phase), revealing an average positron lifetime of 167 ps. This value is lower than the minimum value of $\overline{\tau}$ measured during the isochronal annealing cycles, indicating that thermal vacancies drive the $\overline{\tau}$ variation observed (i. e., C_v).

II. Theoretical calculations of positron lifetimes

Positron lifetime calculations were conducted within the two component density functional theory framework[7, 8]. The annihilation rate λ, which is the inverse of the τ positron lifetime, is evaluated by overlapping the $n_+(\mathbf{r})$ positron and $n_-(\mathbf{r})$ electron densities of the solid

$$\lambda = \tau^{-1} = \pi c r_o^2 \int n_+(\mathbf{r}) n_-(\mathbf{r}) \gamma(\mathbf{r}) \mathrm{d}\mathbf{r} \quad (1)$$

where c is the speed of light in vacuum, r_0 the classical electron radius and $\gamma(\mathbf{r})$ the so-called enhancement factor that comprises the enhanced electron density due to the Coulombic attraction exerted by e^+. The positron lifetime for the perfect (i. e., bulk lifetime) and defected lattice was computed by the Atomic Superposition Approximation (AT-SUP) method[9]. Within this scheme, the electron density $n_-(\mathbf{r})$, is constructed by adding individual atomic n_-^i charge densities around $\mathbf{R_i}$ atomic positions, over all the occupied atomic sites:

$$n_-(\mathbf{r}) = \sum_i n_-^i(|\mathbf{r} - \mathbf{R_i}|). \quad (2)$$

The potential felt by the positron, $V_+(\mathbf{r})$, is constructed as

$$V_+(\mathbf{r}) = V_c(\mathbf{r}) + V_{corr}[n_-(\mathbf{r})], \quad (3)$$

where $V_c(\mathbf{r})$ is the Coulomb potential of the entire crystal and $V_{corr}[n_-(\mathbf{r})]$ the positron-electron correlation potential, which depends on the electron density.

The enhancement factor of Eq. (1) and the correlation potential of Eq. (3) have been taken into account within i) local density approximation (LDA) and ii) Generalized Gradient Approximation (GGA) frameworks. Within the LDA approximation, the $V_{corr}[n_-(\mathbf{r})]$ has been modeled using the interpolation formula proposed by Boronski and Nieminen[8], which is based on the results of Arponen and Pajane[10]. Regarding $\gamma(\mathbf{r})$, calculations have been performed by employing three different parameterizations. First, the expression proposed by Boronski and Nieminen[8], which is based on the many-body calculation by Lantto[11] (labeled as LDA-BN),

$$\gamma(\mathbf{r})^{\mathrm{BN}}_{\mathrm{LDA}} = 1 + 1.23 r_s + 0.8295 r_s^{3/2} - 1.26 r_s^2 + 0.3286 r_s^{5/2} + \frac{1}{6} r_s^3 \quad (4)$$

where $r_s = (3/4\pi n_-)^{1/3}$. The other two expressions proposed by Barbiellini *et al.*[12] are based on results of Arponen and Pajanne[10], which have been labeled as LDA-AP1,

$$\gamma(\mathbf{r})^{\mathrm{AP1}}_{\mathrm{LDA}} = 1 + 1.23 r_s - 0.0742 r_s^2 + \frac{1}{6} r_s^3 \quad (5)$$

and LDA-AP2

$$\gamma(\mathbf{r})^{\mathrm{AP2}}_{\mathrm{LDA}} = 1 + 1.23 r_s - 0.91657 r_s^{3/2} + 1.0564 r_s^2 - 0.3455 r_s^{5/2} + \frac{1}{6} r_s^3. \quad (6)$$

respectively. Within the GGA approximation, both correlation energy and the enhancement factors have been taken into account using the expression proposed by Barbiellini *et al.*[12, 13], which is based on the results of Arponen and Pajanne[10]. In this scheme the $\gamma(\mathbf{r})_{\mathrm{GGA}}$ enhancement factor is deduced from the enhancement factor obtained in the LDA scheme. The effects of the non-uniform electron density are modeled by a parameter $\epsilon = |\Delta \ln n_-|^2 / \mathrm{q}_{TF}^2$. It describes the reduction of the screening cloud close to the positron, being q_{TF} the local Thomas-Fermi screening length. Finally, an adjustable parameter α is also introduced so the corrected enhancement factor then reads,

$$\gamma(\mathbf{r})_{\mathrm{GGA}} = 1 + (\gamma(\mathbf{r})_{\mathrm{LDA}} - 1)\, e^{-\alpha\epsilon}. \quad (7)$$

The value of α is set to be $\alpha = 0.22$, which has been proven to give lifetimes for different types of metals and semiconductors in good agreement with the experimental results[12, 14]. For calculations performed within the GGA approximations, two parameterization for the $\gamma(\mathbf{r})_{\mathrm{GGA}}$ of Eq. (7) were used: i) the expression of Eq. (5) labeled as $\gamma(\mathbf{r})^{\mathrm{AP1}}_{\mathrm{GGA}}$ and ii) the expression of Eq. (6), labeled as $\gamma(\mathbf{r})^{\mathrm{AP2}}_{\mathrm{GGA}}$. It is noteworthy to mention that when $\alpha \to 0$ the Eq. (7) turns into $\gamma(\mathbf{r})_{\mathrm{GGA}} = \gamma(\mathbf{r})_{\mathrm{LDA}}$. $\gamma(\mathbf{r})^{\mathrm{BN}}_{\mathrm{LDA}}$ parameterization gives good account of the experimentally measured lifetimes in the studied Ni-Fe-Ga alloy. However, future works on the implementation of the proposed parameter-free model for $\gamma(\mathbf{r})$[15] and the enhanced electron-positron correlation potential based on quantum Monte Carlo results[16], may shed light on the suitability of other parameterizations for proper lifetime calculations in Ni-Fe-Ga alloys.

The positron lifetime was evaluated at both Γ and L points of the Brillouin zone, as well as calculating the average of the wave functions from Γ and L points. The calculations were performed using the supercell approach accounting for the correct composition of the sample. The supercell corresponding to $Ni_{55}Fe_{17}Ga_{28}$ was built starting from a stoichiometric Ni_2FeGa lattice and by substituting Fe atoms by Ni and Ga atoms[17] until the measured composition of the sample was matched. The antisite atoms were distributed homogeneously. Several configurations of homogeneously distributed antisites were used, giving similar results. Afterwards, in order to overcome artificial defect-defect interactions, caused by periodic boundary conditions, the supercell was built increasing its size in order to ensure the convergence of 0.1 ps in lifetime and 0.01 eV in positron binding energies.

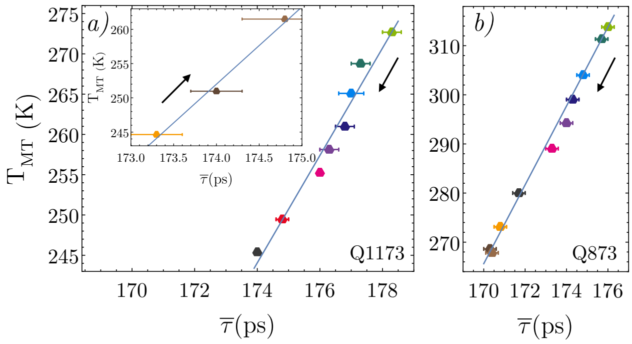

FIG. 2. Mutual relationship between the evolution T_{MT} $\overline{\tau}$ for (a) sample Q1173 and (b) sample Q873.

For the austenite phase a $5\times5\times5$ supercell expansion of the primitive unit cell[18] was created containing 500 atoms, whereas for the martensite phase a $3\times3\times3$ supercell expansion of the primitive unit cell[18] has been used with 108 total atoms. A mesh size of 160^3 was used in the austenite and martensite supercells. Finally, the Schrödinger equation is discretized, and the positron wave function and its energy eigenvalue are solved iteratively at the mesh points of the supercell using a numerical relaxation method[19].

II. Relation between the average positron lifetime and vacancy concentration.

Fig. 2 evinces the mutual dependence of the evolution of T_{MT} and C_v. In sample Q1173, the ordering process during subsequent IAC is accomplished by a reduction of $\overline{\tau}$, which in turn, matches with the T_{MT} decrease (see Fig. 2(a)). Additionally, as shown in the inset of Fig. 2(a), between 550 - 600 K, T_{MT} increases with the $\overline{\tau}$ increase, which takes place at same temperature. Regarding the AQ873 sample, Fig. 2(b) shows, again the mutual relationship between the evolution of T_{MT} and $\overline{\tau}$. As it is discussed below, the evolution of $\overline{\tau}$ reflects directly the evolution of C_v.

When a positron enters in a solid, it loses energy until reaches thermal equilibrium. Thermalization is followed by diffusion through the solid, until the positron annihilates with a surrounding electron. In a defect-free lattice, the positron annihilates from the delocalized state (i.e. Bloch state) at an average rate λ_b or with a characteristic lifetime τ_b. However, solids have imperfections in their lattice, such as vacancies, dislocations, etc. that may act as positron traps. The trapping occurs when a positron turns from the Bloch state into a localized state within a defect (i.e. the positron wave function is localized at the defect). The κ_d trapping rate of a defect is proportional to the defect concentration C_d[20] as

$$\kappa_d = \mu_d C_d. \tag{8}$$

The μ_d parameter is the specific trapping coefficient of the defect and it depends on the type of defect and on the surrounding lattice[21, 22].

When a sample contains different positron states (bulk and defect states) where positrons may annihilate, the statistically strongest parameter obtained from PALS spectra is the average positron lifetime $\overline{\tau}$, which is composed by the different positron annihilation contributions coming from the different positron states in the material[23]. The individual η contributions are weighted so that

$$\overline{\tau} = \eta_b\tau_b + \sum_i \eta_v^i \tau_d^i, \tag{9}$$

where τ_d^i is the lifetime related with i-th defect. Vacancies are the most important traps for positrons in metals. Due to the lack of the positive ion, vacancies act as deep traps for positrons. Vacancies are characterized by an open volume with an electron density lower than the one corresponding to the perfect lattice and, as a consequence according to Eq. (1), they exhibit longer positron lifetimes. Beyond open-volume defects, negatively charged defects without open-volume (e.g., acceptor-type impurities or anti-site defects in semiconductors), can also act as shallow positron trapping centers (ST)[24, 25]. In this case, due to the lack of open volume, the wavefunctions of positrons trapped at ST is extended into the bulk surrounding it. Thus, the expected lifetime of positrons trapped in ST is similar to that of the positrons in a Block state or in a delocalized state. Due to the small binding energy of positrons trapped at Rydberg states, the trapping only occurs well below room temperature[26]. Thus, the contribution of anti-site defect and ST centers at room temperature is negligible.

Considering the presence of a single type of open-volume defect, such as a vacancy, ($\kappa_d = \kappa_v, \tau_d = \tau_v$ and $\mu_d = \mu_v$) Eq. (9) adopts the well-known *one-trap model* form,

$$\overline{\tau} = \tau_b \frac{1+\kappa_v\tau_v}{1+\kappa_v\tau_b} \tag{10}$$

or,

$$\kappa_v = \mu_v C_v = \frac{1}{\tau_b}\frac{\overline{\tau}-\tau_b}{\tau_v-\overline{\tau}} \;\rightarrow\; C_v = \frac{1}{\tau_b\mu_v}\frac{\overline{\tau}-\tau_b}{\tau_v-\overline{\tau}} \tag{11}$$

Eq. (11) evidences the mutual dependency of $\overline{\tau}$ and C_v. Despite that in semiconductors where μ_v may depend on temperature[27], in metals, due to the lack of charge effects, the specific trapping coefficient has a constant value. Additionally, for a given defect in metals, τ_v remains constant and the value of τ_b is determined by the lattice. As a result, in metals (so in Ni-Fe-Ga) the evolution of $\overline{\tau}$ reflects directly the vacancy dynamics.

The vacancy concentration can be estimated by means of Eq. (11). Usually, τ_v and τ_b can be subtracted after decomposing $\overline{\tau}$. However, this decomposition is not always possible and in the saturation trapping regime ($|\overline{\tau} - \tau_v| < 10$) it is unfeasible to decompose the spectra[23]. However, if the theoretically calculated τ_v and τ_b values are compatible with the experimental results, Eq. (11) can be used to estimate the C_v concentration.

* iraultza.unzueta@ehu.eus

[1] J. M. Barandiarán, V. A. Chernenko, P. Lázpita, J. Gutiérrez, and J. Feuchtwanger, Phys. Rev. B **80**, 104404 (2009).
[2] P. Kirkegaard and M. Eldrup, Comput. Phys. Commun. **7**, 401 (1974).
[3] M. Bertolaccini and L. Zappa, Il Nuovo Cimento B Series 10 **52**, 487 (1967).
[4] B. Somieski, T. Staab, and R. Krause-Rehberg, Nucl. Instrum. Method. A. **381**, 128 (1996).
[5] K. Plotkowski, T. Panek, and J. Kansy, Il Nuovo Cimento D **10**, 933 (1988).
[6] I. MacKenzie and J. Fabian, Il Nuovo Cimento B **58**, 162 (1980).
[7] R. M. Nieminen, E. Boronski, and L. J. Lantto, Phys. Rev. B **32**, 1377 (1985).
[8] E. Boroński and R. M. Nieminen, Phys. Rev. B **34**, 3820 (1986).
[9] M. J. Puska and R. M. Nieminen, J. Phys. F: Met. Phys **13**, 333 (1983).
[10] J. Arponen and E. Pajanne, Ann. Physics **121**, 343 (1979).
[11] L. J. Lantto, Phys. Rev. B **36**, 5160 (1987).
[12] B. Barbiellini, M. J. Puska, T. Torsti, and R. M. Nieminen, Phys. Rev. B **51**, 7341 (1995).
[13] B. Barbiellini, M. J. Puska, T. Korhonen, A. Harju, T. Torsti, and R. M. Nieminen, Phys. Rev. B **53**, 16201 (1996).
[14] J. M. C. Robles, E. Ogando, and F. Plazaola, J. Phys. Condens. Matter **19**, 176222 (2007).
[15] B. Barbiellini and J. Kuriplach, Phys. Rev. Lett. **114**, 147401 (2015).
[16] N. D. Drummond, P. López Ríos, R. J. Needs, and C. J. Pickard, Phys. Rev. Lett. **107**, 207402 (2011).
[17] J. Bai, Y. Chen, Z. Li, P. Jiang, P. Wei, and X. Zhao, AIP Adv. **6**, 125007 (2016).
[18] P. J. Brown, A. P. Gandy, K. Ishida, R. Kainuma, T. Kanomata, H. Morito, K.-U. Neumann, K. Oikawa, and K. R. A. Ziebeck, J. Phys. Condens. Matter **19**, 016201 (2007).
[19] G. E. Kimball and G. H. Shortley, Phys. Rev. **45**, 815 (1934).
[20] W. Brandt and R. Paulin, Phys. Rev. B **5**, 2430 (1972).
[21] P. Hautöjarvi, *Positrons in Solids. Topics in Current Physics*, Vol. 12 (Springer, Heidelberg, 1979).
[22] M. Puska and R. Nieminen, Rev. Mod. Phys. **66**, 841 (1994).
[23] F. Tuomisto and I. Makkonen, Rev. Mod. Phys. **85**, 1583 (2013).
[24] K. Saarinen, P. Hautojärvi, A. Vehanen, R. Krause, and G. Dlubek, Phys. Rev. B **39**, 5287 (1989).
[25] C. Corbel, F. Pierre, K. Saarinen, P. Hautojärvi, and P. Moser, Phys. Rev. B **45**, 3386 (1992).
[26] F. Plazaola, K. Saarinen, L. Dobrzynski, H. Reniewicz, F. Firszt, J. Szatkowski, H. Meczynska, S. Legowski, and S. Chabik, J. Appl. Phys. **88**, 1325 (2000).
[27] R. Krause-Rehberg, A. Polity, W. Siegel, and G. Kuhnel, Semicond. Sci. Tech. **8**, 290 (1993).